Using atomic interference to probe atom-surface interactions

Roberta Marani, Laurent Cognet, Veronique Savalli, Nathalie Westbrook, Christoph I. Westbrook, and Alain Aspect
Laboratoire Charles Fabry de l'Institut d'Optique, Unité Mixte du CNRS no. 8501, BP 147, 91403 Orsay Cedex, France
(Received 3 November 1999; published 6 April 2000)

We show that atomic interference in the reflection from two suitably polarized evanescent waves is sensitive to retardation effects in the atom-surface interaction for specific experimental parameters. We study the limit of short and long atomic de Broglie wavelengths. The former case is analyzed in the semiclassical approximation (Landau-Zener model). The latter represents a quantum regime and is analyzed by solving numerically the associated coupled Schrödinger equations. We consider a specific experimental scheme and show the results for rubidium (short wavelength) and the much lighter metastable helium atom (long wavelength). The merits of each case are then discussed.

PACS number(s): 42.50.Vk, 34.20.−b, 32.80.Lg, 03.75.−b

I. INTRODUCTION

The interaction between a ground-state atom and a dielectric or conducting wall has been investigated theoretically [1–10] and experimentally [11–14]. Theoretical studies have been performed on different levels, from a simple model of a dipole-dipole interaction of the atom and its mirror image, to the full QED relativistic quantum treatment. Interesting in particular are the long-range Casimir interactions [6] that were recently observed in cavity QED experiments [13,14]. When the atom-wall distance z is not small compared to the wavelength of the dominant atomic transitions, the z^{-3} law associated with the instantaneous electrostatic interaction is no longer valid. The full QED treatment leads to the famous long-distance z^{-4} law.

Recent experimental developments enable precise manipulation of cold atoms by lasers, see, e.g., Ref. [15]. Small and well defined velocities of the atoms can be achieved using advanced cooling and launching techniques and a detuned laser field can be used to create controlled and adjustable potentials for the atoms. Under these conditions, atoms can be used to explore the atom-surface potential, for example, using evanescent-wave mirrors. Classical reflection from such an atomic mirror was used to measure the van der Waals force between a dielectric surface and an atom in its ground state [11]. This experiment though, could not fully discriminate between the electrostatic and the QED expressions. Segev *et al.* [16] considered a similar experiment in the quantum regime (atoms undergoing above-barrier, classically forbidden reflection). Unlike classical reflection, which can only be used to identify thresholds and to measure the height of the potential barrier, quantum probabilities are determined by the complete potential curve, and are sensitive to the short- and long-range behavior of the potential. It was found that, for velocities of the order of the recoil speed, the quantum reflection probabilities are indeed sensitive to the long-range (Casimir) interaction.

In this work we study how the form of the atom-surface interaction can be observed using atomic interference of the type reported in Ref. [17]. We consider atoms with multiple ground-state sublevels, which feel different potentials in the evanescent radiation field. These potentials can be probed by using stimulated Raman transitions within the evanescent wave. These transitions exhibit interference effects whose phases depend on the atomic trajectories and on the entire potential, as in quantum reflection. An important aspect of the effects we discuss here is that they occur for higher incident velocities than those considered in Ref. [16] and may therefore be experimentally easily accessible. Furthermore, even for small velocities (near the recoil velocity) the effects are more dramatic than those shown by quantum reflection.

As discussed in Refs. [18] and [17], the experiment is analogous to an atom interferometer whose size is of the order of a fraction of the evanescent wave decay length, κ^{-1}. We will focus on three experimental cases: in the first, the atomic de Broglie wavelength $\lambda_{dB} \ll \kappa^{-1}$. This leads to interference fringes analogous to those in any other interferometer. It corresponds to the experiment described in Ref. [17] in which rubidium (Rb) atoms are dropped from a height of about 2 cm. Second, we will repeat the situation of the first case, but with Rb replaced by metastable helium (He*). In this case we have $\lambda_{dB}/2\pi \simeq$ a few κ^{-1}, which allows for only a few interference fringes. This allows us to illustrate how the signal changes when only the atomic species is changed. Finally, we will examine the case where $\lambda_{dB}/2\pi \simeq \kappa^{-1}$, taking He* atoms at the recoil velocity as our example. No fringes are present, but a strong dependence on the nature of the atom-wall potential is demonstrated. To simplify the discussion, we work with a two-level model, between the initial atomic state and the adjacent one in the ground-state manifold, thus neglecting the populations of the other ground state sublevels as well as the excited levels. For the atom-wall interaction we will use the published values for each atom.

In the short λ_{dB} limit, the motion of the atom can be treated semiclassically. We thus calculate the transition probability between the two atomic levels according to the Landau-Zener model for adiabatic transitions. In the other cases, the study of the atomic motion requires a fully quantum-mechanical treatment. We study these cases by solving the associated coupled Schrödinger equations numerically.

In Sec. II we describe the physical system and the theory for atomic interference. In Sec. III the results are presented. Discussion and conclusions are given in Sec. IV.

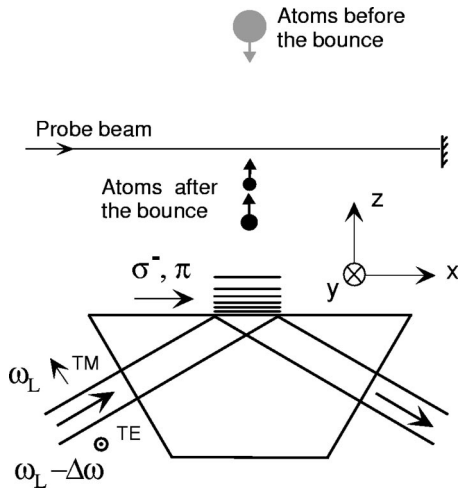

FIG. 1. Typical experimental setup. The atoms are released from a magneto-optical trap above the prism. Two slightly detuned laser beams of polarizations TM [and frequency $\omega/(2\pi)$] and TE [and frequency $(\omega-\Delta\omega)/(2\pi)$] form evanescent waves on the surface of the prism of polarizations σ^- and π, respectively (y is the quantization axis). The reflected atoms are detected by a detection beam.

II. MODEL FOR INTERFERENCE OF MULTIPLE GROUND-STATE SUBLEVELS

We will focus on an experimental setup along the lines of Fig. 1. Here, a strong laser beam with frequency ω and transverse magnetic (TM) polarization (i.e., magnetic field perpendicular to the plane of incidence) creates an evanescent wave, which is nearly σ^- circularly polarized with respect to the y axis. A second weak laser beam with frequency $\omega-\Delta\omega$ and transverse electric (TE) polarization (i.e., electric field perpendicular to the plane of incidence) creates another evanescent wave with π polarization along the y axis.

Atoms normally incident on the evanescent wave move in an effective optical potential $\hat{V}_{\rm light}$ (which in general depends on the internal state of the atom) and an attractive atom-wall interaction $\hat{V}_{\rm wall}$. The total potential is given by

$$\hat{U}(z)=\hat{V}_{\rm light}(z)+\hat{V}_{\rm wall}(z). \tag{1}$$

A. Optical potential

Let us consider an atom in the evanescent field and assume for simplicity that the σ^- polarized wave is strong compared to the π wave. The σ^- component lifts the magnetic (Zeeman) degeneracy of the atomic ground state (the quantization axis is in the $\hat{y}$ direction), so that each magnetic sublevel feels a different optical potential. To first order, the π polarized wave produces a coupling between the atomic sublevels via a Raman transition: for example, starting from the sublevel m_i, the atom absorbs a σ^- polarized photon and emits a stimulated photon with π polarization. The atom thus ends up in the m_i-1 substate with its total energy increased by $\hbar\Delta\omega$. This transition is resonant when $\hbar\Delta\omega$ is equal to the energy difference between the magnetic sublevels. If the two evanescent waves are counterpropagating, in the reference frame moving with the optical grating, the situation corresponds to grazing incidence diffraction [17]. For a review of the theoretical understanding of atomic diffraction and interference from evanescent waves, see Ref. [19].

In the limit of low saturation and a detuning δ large compared to both the frequency difference $\Delta\omega$ and the natural linewidth, the excited state manifold may be eliminated adiabatically, and, for a ground state of total angular momentum (including nuclear spin) J_g, the atomic wave function is described by the $2J_g+1$ Zeeman components $|m\rangle, m=-J_g,\ldots,+J_g$. An atom at a distance z from the surface of the mirror is subject to an optical potential $\hat{V}_{\rm light}(z)$ whose matrix elements are of the form [we suppose that the frequency difference $\Delta\omega$ and Zeeman shift are negligible compared to the detuning δ and the hyperfine structure of the excited level]

$$\langle m|\hat{V}_{\rm light}(z)|m'\rangle=\frac{d^2}{\hbar\delta}\sum_{q,q',m_e,J_e}E_q^*(z)E_{q'}(z)\times(J_g m;1q|J_e m_e)(J_e m_e|J_g m';1q'), \tag{2}$$

where a product of Clebsch-Gordon coefficients appears on the right-hand side, the electric field polarization is expanded in the usual spherical basis with coefficients E_q, $(q=-1,0,+1)$, and d is the reduced dipole moment. The optical potential couples different Zeeman sublevels if the field is not in a pure polarization state with respect to this basis, as in the setup considered in this work. The optical potential due to the two evanescent waves can then be written as

$$\langle m|\hat{V}_{\rm light}(z)|m'\rangle=\frac{d^2}{\hbar\delta}C_{mm'}\exp(-2\kappa z), \tag{3}$$

where the $C_{mm'}$ coefficients are given by the Clebsch-Gordon coefficients times the field amplitudes at the surface $z=0$ [see Eq. (2)]. The inverse decay length κ is $\kappa=k[(n\sin\theta)^2-1)]^{1/2}$, where $k=\omega/c$ is the free field wave vector, assumed to be the same for each laser, n is the refraction index of the prism and θ is the angle of incidence of the lasers with the surface. In our calculations we will always use $n=1.87$ and $\theta=53°$. The wave vector k is different for each atom.

B. Atom-wall potential

The simplest model for the interaction of a ground-state atom and a wall of dielectric constant ϵ considers the interaction between a dipole **d** and its mirror image and yields the Lennard-Jones potential,

$$V_{\rm wall}^{\rm LJ}(z)=-\frac{\epsilon-1}{\epsilon+1}\left(\frac{\langle d_\parallel^2\rangle+2\langle d_\perp^2\rangle}{64\pi\epsilon_0}\right)\frac{1}{z^3}\equiv-\frac{\epsilon-1}{\epsilon+1}\frac{C^{(3)}}{z^3}, \tag{4}$$

where $\langle d_\parallel^2\rangle$ and $\langle d_\perp^2\rangle$ are the expectation values of the squared dipole parallel and perpendicular to the surface [1],

TABLE I. Values of parameters used in the text for Rb and He*: laser wavelength λ, atomic transition width Γ, recoil energy E_r, van der Waals coefficient $C^{(3)}$ [see Eq. (4)]. Definition of the initial and final atomic state (i and f). Optical potential coefficients C_{ij} [see Eq. (3)]. We assume here that the σ^- wave (E_{-1}) is much stronger than the π wave (E_0). The dielectric constant of the wall is $\epsilon=3.49$ and $\kappa=1.52k$. (The asterisk denotes the complex conjugate.)

Parameter	Rb	He*
λ	780×10^{-9} m	1083×10^{-9} m
Γ	$2\pi 5.9\times10^{6}$ s^{-1}	$2\pi 1.6\times10^{6}$ s^{-1}
E_r	$6.4\times10^{-4}\hbar\Gamma$	$2.6\times10^{-2}\hbar\Gamma$
$C^{(3)}$	$0.113\hbar\Gamma/\lambda^3$	$0.125\hbar\Gamma/\lambda^3$
state i	$5S_{1/2},F=2,m_F=2$	$2^3S_1,J=1,m_J=1$
state f	$5S_{1/2},F=2,m_F=1$	$2^3S_1,J=1,m_J=0$
C_{ii}	$\frac{1}{3}\lvert E_{-1}(0)\rvert^2$	$\frac{1}{6}\lvert E_{-1}(0)\rvert^2$
C_{ff}	$\frac{1}{2}\lvert E_{-1}(0)\rvert^2$	$\frac{1}{2}\lvert E_{-1}(0)\rvert^2$
C_{if}	$E^*_{-1}(0)E_0(0)\sqrt{2}/3$	$\frac{1}{3}E^*_{-1}(0)E_0(0)$

[20]. This expression for the potential is approximately valid for ϵ independent of frequency and kz much smaller than unity.

If we take into account retardation effects, the Casimir-Polder potential is obtained, where the finite propagation time between the dipole and its image results in a different power-law behavior for large z [2],

$$\lim_{z\to\infty} V^{\mathrm{CP}}_{\mathrm{wall}}(z)\propto z^{-4}. \tag{5}$$

In the complete QED theory the interaction potential between an atom of polarizability $\alpha(\omega)$ at a distance z from a dielectric wall can be written as [5]

$$V^{\mathrm{QED}}_{\mathrm{wall}}(z)=-\frac{\hbar}{8\pi^2c^3}\int_0^\infty d\omega\omega^3\alpha(\omega) \times\left(\int_0^1 dp+\int_0^{i\infty} dp\right)H(p,\epsilon)\exp(-2ip\omega z/c) \tag{6}$$

with

$$H(p)=\frac{\sqrt{\epsilon-1+p^2}-p}{\sqrt{\epsilon-1+p^2}+p}+(1-2p^2)\frac{\sqrt{\epsilon-1+p^2}-\epsilon p}{\sqrt{\epsilon-1+p^2}+\epsilon p}. \tag{7}$$

The numerical values of the constant $C^{(3)}$ for Rb and He* atoms used in this paper are given in Table I, as well as the numerical values of some other important parameters. Since the atom is in a ground state with $l=0$, the value of $C^{(3)}$ is the same for any magnetic or hyperfine sublevel. The detailed interaction between a ground-state Rb or metastable He atom and a dielectric surface were recently calculated. For the van der Waals potential we have used data from Ref. [21] for Rb and from Ref. [22] for He*. In the former work an interpolation formula for the van der Waals potential is given as $V^{\mathrm{QED}}_{\mathrm{wall}}(z)=V^{\mathrm{LJ}}_{\mathrm{wall}}(z)0.987[(1+1.098z)^{-1}-0.00493z(1+0.00987z^3-0.00064z^4)^{-1}]$ where z is expressed in units of the laser wavelength $\lambda/(2\pi)$. This formula approximates the numerical calculation with a 0.6% accuracy between 0 and $10\lambda/(2\pi)$.

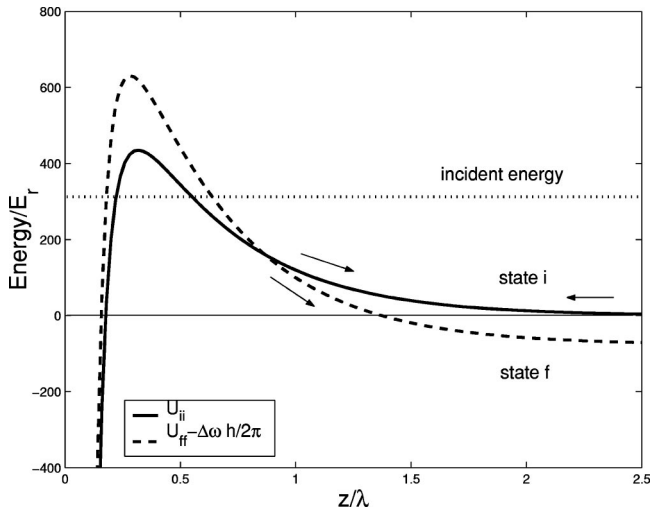

FIG. 2. Typical potential curves experienced by the atoms during reflection. The potential for state f is shifted by the Raman energy $-\hbar\Delta\omega$. The atoms approach the potential barrier in state i, pass through the curve crossing twice and can end up on either state i or f. For each final situation, two paths are possible (between the crossing and the turning points) and can interfere producing fringes as a function of the location of the crossing.

C. Population transfer

In this work we will consider only population transfer from the incident sublevel i to the final one f ($m_f=m_i-1$), that is only two levels. This is a good approximation if the coupling is weak enough for the population of the other levels to be negligible. An example of the total interaction potential from Eq. (1) is shown in Fig. 2. The U_{ff} potential curve has been shifted vertically by $-\hbar\Delta\omega$, corresponding to the kinetic energy change. Then the two (adiabatic) potential curves cross at the point of resonance. The coupling turns the exact crossing into an avoided crossing. An incoming wave function in the m_i channel is split in two parts that are subsequently reflected from their respective repulsive potentials and recombined after the second passage at the crossing. Thus, the evanescent wave realizes a ''Michelson interferometer'' with a single beam splitter and two mirrors.

When the atomic λ_{dB} is short, the avoided crossing can be treated by means of the semiclassical Landau-Zener model for nonadiabatic transitions [23]. Assuming that the atom moves through the crossing with a constant velocity v_c (fixed by energy conservation), the Landau-Zener formula allows one to compute the probability amplitude for the two atomic levels after the crossing. The transition probability w_{if} from the initial sublevel i to the final sublevel f is given by

$$w_{i,f}=4T_{LZ}R_{LZ}\cos^2(\delta\phi), \tag{8}$$

where $R_{LZ}=1-T_{LZ}$ and the transmission coefficient is $T_{LZ}=\exp(-\pi\Lambda)$, with $\Lambda=2|\langle i|\hat{U}|f\rangle|^2/(\hbar^2\kappa\Delta\omega v_c)$.

The phase difference $\delta\phi$ is given by the difference in the phase shifts between the crossing and the turning points in the semiclassical approximation, plus a correction term [24]:

$$\delta\phi=\frac{1}{\hbar}\left[\int_{z_{f,r}}^{z_c}dz p_f(z)-\int_{z_{i,r}}^{z_c}dz p_i(z)\right]+\frac{\pi}{4}+\frac{\Lambda}{2}\log\left(\frac{\Lambda}{2e}\right)+\arg\left[\Gamma\left(1-i\frac{\Lambda}{2}\right)\right], \tag{9}$$

where z_c is the position of the crossing point, $z_{n,r}$ the classical return point for an atom in the nth level, $p_n(z)$ its momentum, and Γ the gamma function.

Changing the frequency difference $\Delta\omega/(2\pi)$ causes a change in the length of one of the interferometer arms, thus a change in the phase difference $\delta\phi$ between the two paths. As a consequence we expect the transition probability to show oscillations in $\Delta\omega$ (Stückelberg oscillations). We will see in the next section that $\delta\phi$ is very sensitive to the exact shape of the potential. The amplitude of the oscillations also depends on $\Delta\omega$ both explicitly and implicitly through v_c (the crossing point moves with changing $\Delta\omega$).

The Landau-Zener model is a good approximation only when the atom speed is approximately constant during the crossing. In particular it is not valid when the classical return point and the crossing are close to each other or when the de Broglie wavelength of the atom is of the order of the width of the interaction region. In order to explore this long-wavelength regime, we have to forgo the semiclassical Landau-Zener model and solve numerically the coupled Schrödinger equations for the system. Since atoms that cross the potential barrier stick to the dielectric surface, the appropriate boundary conditions at the surface are those for a running wave propagating downward ($z\rightarrow-\infty$), while for $z\rightarrow\infty$ the solution is a superposition of downward (incident) and upward (reflected) waves. We have integrated the system of Schrödinger equations using the renormalized Numerov method [25]. To avoid the singularity at the surface we have modified the potential to be a large negative constant near the interface and verified that the transition probability does not change by varying the value of the constant.

III. RESULTS

We will present our calculations in two parts. First we discuss the short-wavelength regime, and point out various experimental strategies to observe retardation effects. Then we discuss two cases in which the de Broglie wavelength is not small compared to the evanescent wave decay length (the ''long-wavelength regime''), in which a numerical integration of the Schrödinger equation is necessary.

A. Short-wavelength regime

Figure 3 shows a calculation of the population transfer w_{if} as a function of the frequency difference $\Delta\omega$ for the Lennard-Jones (LJ) and QED model of the van der Waals interaction. The value of the light potential is the same for the two curves (i.e., the laser intensity is the same), and the incident momentum is $115\hbar k$, which corresponds to Rb atoms dropped from a height of 2.3 cm. We use the Landau-Zener approach to calculate the transfer probability [see Eq. (8)]. As in Refs. [18] and [17], we observe Stückelberg oscillations in the transfer probability. These oscillations can be understood as the variations in the accumulated phase difference between the two different paths taken by the atoms after the level crossing shown in Fig. 2. The de Broglie wavelength λ_{dB} is such that several fringes appear as the position of the level crossing is moved through its possible range. The last oscillation at the higher frequencies is where the crossing point and the classical return point are very close to each other and the Landau-Zener model breaks down. We have set the probability to zero beyond this limit. In reality, the transition probability falls roughly exponentially with frequency, as one finds solving the Schrödinger equations numerically (see next subsection).

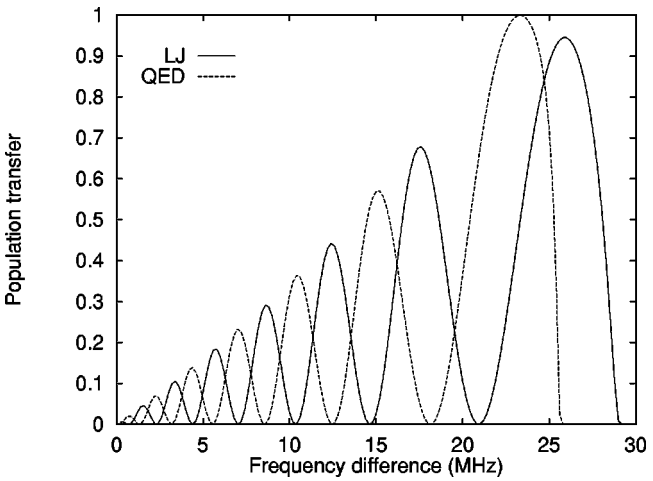

FIG. 3. Population transfer from state i to state f after reflection [w_{if} from Eq. (8)] vs frequency difference $\Delta\omega/(2\pi)$ for rubidium atoms, released 2.3 cm above the mirror, (i.e., with incident momentum $115\hbar k$). The solid line is for the QED model and the dashed line for the LJ model. The coupling coefficients defined in Eq. (3) are $|C_{if}|=859E_r^{\mathrm{Rb}}$ and $|C_{ii}|=3.8\times10^4E_r^{\mathrm{Rb}}$.

In general, we find that the dephasing between the two curves (with and without retardation effects) is greatest when the atoms are incident at an energy close to the top of the potential barrier. Note that the height of the barrier is greater when retardation effects are included, since these reduce the strength of the atom-surface interaction. The effect of retardation is roughly to shift these fringes by half a fringe to the left. The major cause of this shift is the increase in the height of the total potential which is greater for the i level than the f level. A 10% increase in the value of the light-shift potential would exhibit nearly the same shift. Therefore, since it is not possible to turn retardation on and off, it would be necessary to measure absolutely the light-shift potential to better than 10% in order to distinguish a retardation effect. Experimentally this is rather difficult. Instead of attempting to measure the absolute light shift, one could rather measure the absolute height of the potential by observing the threshold of

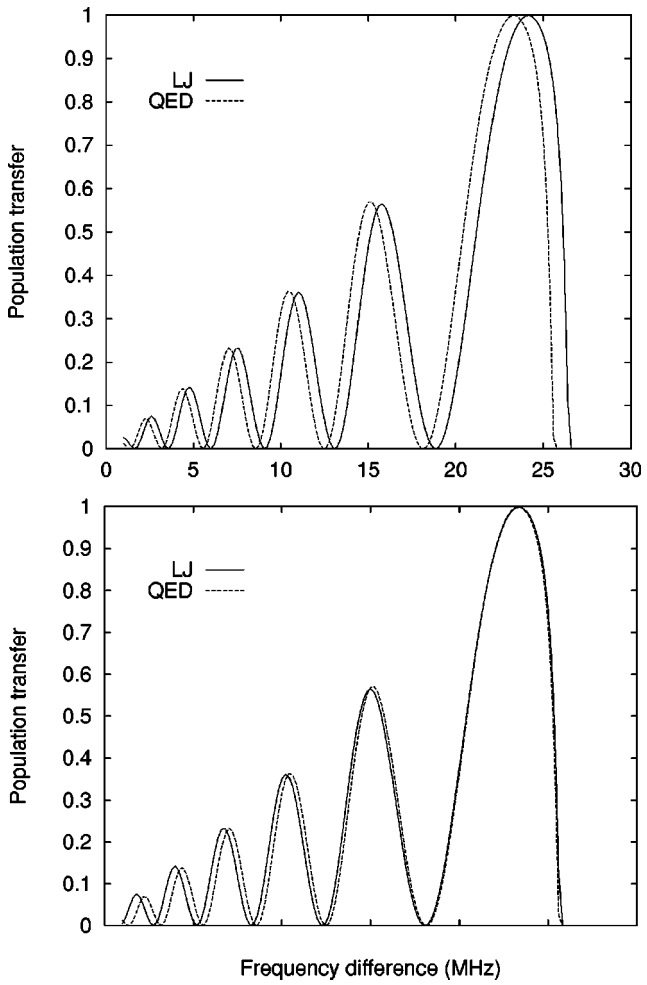

FIG. 4. Upper figure: population transfer w_{if} [see Eq. (8)] vs frequency difference $\Delta\omega/(2\pi)$ for rubidium atoms released 2.3 cm above the mirror (i.e., with incident momentum $115\hbar k_{\mathrm{Rb}}$). The solid line is for the QED model and the dashed line for the LJ model. The height of the potential barrier is $1.48\times10^4 E_r^{\mathrm{Rb}}$, i.e., the intensity of the strong laser beam has been adjusted to give the same barrier height for both models. The light-shift coefficients for the QED model are the same as for Fig. 3, while for the LJ model $|C_{ii}|=4.11\times10^4 E_r^{\mathrm{Rb}}$ and $|C_{if}|=890E_r^{\mathrm{Rb}}$. Lower figure: same parameters as in the previous figure with the LJ curve artificially shifted 0.79 MHz to the left in order to show the changes in fringe spacing.

reflection as in Ref. [11], and using the known kinetic energy of the atoms to get an absolute calibration of the height. Let us assume then that the barrier height, instead of the light intensity, is known. In Fig. 4(a) we show the result with the same parameters as in Fig. 3 except for the light intensity in the LJ model, which has been changed so as to have the same barrier height as the QED model. In this case the shift is much smaller, about 1/5 of a fringe. We have verified that even taking into account an experimental uncertainty of a few percent in the height of the corresponding potentials, the two models are still clearly resolved.

This approach seems feasible, but a third method of observing the effects of retardation is possible if one uses more of the information available in the oscillation curve. Figure 4(b) shows the same curves as Fig. 4(a) but with the QED curve numerically shifted so as to coincide with the LJ curve at its maximum. One sees that the period of these oscillations is not the same. It decreases with decreasing detuning, faster for the full QED potential, so that there is a difference in the spacing of the minima in the population transfer. Thus with fringes with sufficiently high signal to noise, one can distinguish retardation while leaving the absolute barrier height as a free parameter in a fit to the data. It seems to us that a viable experimental method is to use a combination of the second two approaches. Careful measurements of the barrier height can be used to cross-check a fit to the Stückelberg oscillations with the barrier height as a free parameter.

The incident energy, momentum, and barrier height used in Figs. 3 and 4(a) were arbitrarily chosen to correspond to the experiment in Ref. [17], but it would be interesting to know how Figs. 3 and 4(a) would change, especially for different incident momenta (de Broglie wavelengths). We studied this question by repeating the calculation of Fig. 4(a), for different incident momenta, while always keeping the barrier height 10% above the incident kinetic energy. We find that, roughly speaking, the number of oscillations increases as the incident momentum. This is because the number of fringes in the interferogram increases with decreasing wavelength. The accumulated phase difference between the oscillations in the LJ and QED models, over the corresponding frequency range, also increases approximately linearly with incident momentum. Thus if we consider the fringe shift divided by the fringe period as a figure of merit, the sensitivity of the experiment to retardation effects increases with increasing incident momentum.

B. Long-wavelength regime

We now examine the large de Broglie wavelength limit, where the semiclassical model breaks down since the atomic wavelength is not small compared to the interferometer size. We first consider the case of He* atoms dropped from a height of a few cm as for Rb. We show the results in Fig. 5. For an initial distance of 2.3 cm from the mirror, the incident momentum of He* is $7.4\hbar k$, much lower than for Rb. Again we will chose the intensities of the strong σ^- wave so as to have the same barrier height for the two potentials, about 10% above the incident kinetic energy. In this regime, to observe interference, the detuning between the evanescent waves must be of only a few MHz, in fact, beyond about 10 MHz the crossing point is closer to the surface than the return point. One only sees one or two Stückelberg oscillations since the momentum involved is small and the atoms do not accumulate enough phase difference to show more oscillations. The two potentials give similar results (Fig. 5), the main difference being in the shape and height of the big peak.

We have also looked at even lower incident momenta. Near the recoil limit, one can expect interference only for detunings of less than one MHz and the accumulated phase difference is too small in this range to show any Stückelberg oscillations. Both for He* and Rb one obtains a big peak in the transition probability and no Stückelberg oscillations, as

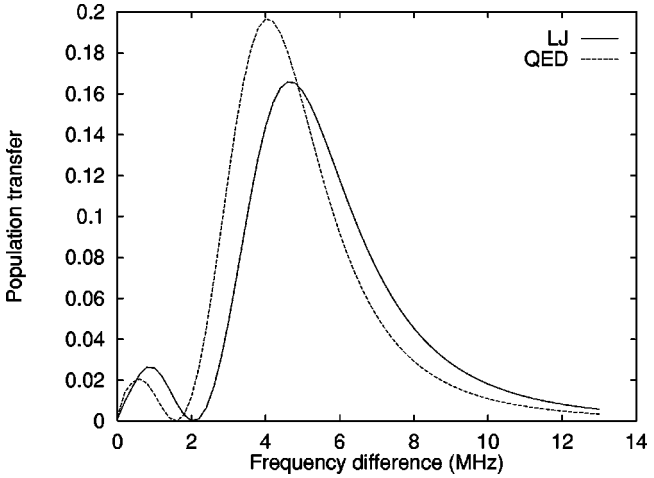

FIG. 5. Population transfer w_{if} [see Eq. (8)] vs frequency difference $\Delta\omega/(2\pi)$ for metastable helium atoms released 2.3 cm above the mirror (i.e., with incident momentum $7.4\hbar k_{\mathrm{He}}$). The solid line is for the QED model and the dashed line for the LJ model. The height of the potential barrier is $61E_r^{\mathrm{He}}$, i.e., the intensity of the strong laser beam has been adjusted to give the same barrier height for both models (10% above the incident kinetic energy). The light-shift coefficients for the QED model are $|C_{ii}|=252E_r^{\mathrm{He}}$ $|C_{if}|=20.8E_r^{\mathrm{He}}$ while for the LJ model $|C_{ii}|=303E_r^{\mathrm{He}}$ and $|C_{if}|=22.7E_r^{\mathrm{He}}$.

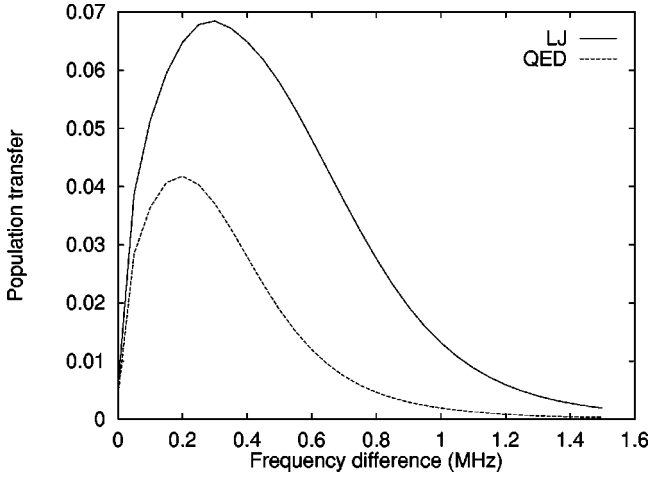

FIG. 6. Population transfer w_{if} vs frequency difference $\Delta\omega/(2\pi)$ for metastable helium atom with incident momentum $\hbar k_{\mathrm{He}}$. The solid line is for the QED model and the dashed line for the LJ model. The height of the potential barrier is $1.28E_r^{\mathrm{He}}$, i.e., the intensity of the strong laser beam has been adjusted to give the same barrier height for both models. The light-shift coefficients for the QED model are $|C_{ii}|=0.8E_r^{\mathrm{He}}$ $|C_{if}|=0.16E_r^{\mathrm{He}}$ while for the LJ model $|C_{ii}|=1.47E_r^{\mathrm{He}}$ and $|C_{if}|=0.29E_r^{\mathrm{He}}$.

expected. The difference between the van der Waals potential and the full QED potential still shows up in the different shape and height of the peaks (Fig. 6). Here the width of the curve is delimited by the frequency for which the classical return point and the crossing point coincide.

Finally we note that the qualitative features of the short and long λ_{dB} limit are the same for Rb and He*, e.g., He* with an incident momentum of about $100\hbar k$ gives the same type of oscillation pattern as Rb.

IV. CONCLUSIONS

In summary, we have proposed an experiment to probe van der Waals-like surface interactions by exploiting interference mechanisms for well defined Zeeman sublevels of atoms moving in two evanescent waves. Retardation can be resolved using atoms incident at speeds which are easily obtained in free fall over a few centimeters. The controlling parameter is here the detuning between the two evanescent waves. One then measures the fraction of the atoms which have undergone a change of magnetic sublevel as a function of this detuning.

For the situation in which the atomic de Broglie wavelength is sufficiently small the experiment resembles typical interferometry experiments. The theoretical description is semiclassical, employing well defined atomic trajectories, while experimentally, one seeks a particular (nonsinusoidal) fringe pattern as a signature of retardation. This should be possible with an improved version of the experiment of Ref. [17].

Another approach is to investigate the interaction of atoms whose de Broglie wavelength is not small compared to the length scale of the interferometer. In this regime most of the information is to be found in the shape of the population transfer curve, since there are very few or zero interference fringes. Note though, that we have assumed throughout that the incident atoms are monoenergetic. This means that the velocity spread of the incident atoms must be small compared to the atomic recoil. Nevertheless this may be worth the effort, because the predicted effect of retardation is quite dramatic.

For a quantitative comparison however, the presence of all the sublevels (which give rise to the multiple crossing of the dressed potentials at the same distance z_c from the surface) and, possibly, losses from spontaneous emission have to be taken into account, but the results are not qualitatively different.

Note added in proof. Recently we have become aware of an article that discusses a closely related interferometry experiment to probe atom-surface interactions [26].

ACKNOWLEDGMENTS

R.M. acknowledges support from the Training and Mobility of Researchers Programme (European Union Contract No. ERBFMBIC983271) and would like to thank Paul Julienne and Olivier Dulieu for their help with the numerical code and J. Babb for providing the data for the atom-wall interaction for metastable helium. This work was also supported by the Région Ile de France.

[1] L. E. Lennard-Jones, Trans. Faraday Soc. **28**, 333 (1932).
[2] H. B. G. Casimir and D. Polder, Phys. Rev. **73**, 360 (1948).
[3] I. E. Dzyaloshinskii, E. M. Lifshitz, and L. P. Pitaevskii, Adv. Phys. **10**, 165 (1961).
[4] L. Spruch and Y. Tikochinsky, Phys. Rev. A **48**, 4213 (1993).
[5] Y. Tikochinsky and L. Spruch, Phys. Rev. A **48**, 4223 (1993).
[6] L. Spruch, Science **272**, 1452 (1996).
[7] M. Fichet, F. Schuller, D. Bloch, and M. Ducloy, Phys. Rev. A **51**, 1553 (1995), and references therein.
[8] J. M. Wylie and J. E. Sipe, Phys. Rev. A **30**, 1185 (1984).
[9] J. M. Wylie and J. E. Sipe, Phys. Rev. A **32**, 2030 (1985).
[10] C. Mavroyannis, Mol. Phys. **6**, 593 (1963).
[11] A. Landragin *et al.*, Phys. Rev. Lett. **77**, 1464 (1996).
[12] M. Kasevich *et al.*, in *Atomic Physics 12*, edited by J. C. Zorn and R. R. Lewis, AIP Conf. Proc. 233 (AIP, New York, 1991), p. 47.
[13] C. I. Sandoghdar, V. Sukenik, E. A. Hinds, and S. Haroche, Phys. Rev. Lett. **68**, 3432 (1992).
[14] C. I. Sukenik *et al.*, Phys. Rev. Lett. **70**, 560 (1993).
[15] S. Chu, C. N. Cohen-Tannoudji, and W. D. Phillips, Rev. Mod. Phys. **70**, 685 (1998).
[16] B. Segev, R. Côté, and M. G. Raizen, Phys. Rev. A **56**, R3350 (1997).
[17] L. Cognet *et al.*, Phys. Rev. Lett. **81**, 5044 (1998).
[18] C. Henkel, K. Molmer, R. Kaiser, and C. I. Westbrook, Phys. Rev. A **56**, R9 (1997).
[19] C. Henkel *et al.*, Appl. Phys. B: Lasers Opt. **69**, 277 (1999).
[20] R. Côté, B. Segev, and M. G. Raizen, Phys. Rev. A **58**, 3999 (1998).
[21] A. Landragin, Ph.D. thesis, Université de Paris-Sud, 1997.
[22] Z.-C. Yan and J. F. Babb, Phys. Rev. A **58**, 1247 (1998).
[23] C. Zener, Proc. R. Soc. London, Ser. A **137**, 696 (1932).
[24] A. P. Kazantsev, G. A. Ryabenko, G. Surdutovich, and V. Yakovlev, Phys. Rep. **129**, 75 (1985).
[25] B. R. Johnson, J. Chem. Phys. **67**, 4086 (1977).
[26] M. Gorlicki, S. Feron, V. Lorent, and M. Ducloy, Phys. Rev. A **61**, 013603 (2000).